An Extended Bidomain Framework Incorporating Multiple Cell Types

Martin L. Buist[†‡*] and Yong Cheng Poh[†‡]
[†]Division of Bioengineering, National University of Singapore, Singapore; and [‡]National University of Singapore Graduate School for Integrative Sciences and Engineering, Singapore

ABSTRACT The muscular layers within the walls of the gastrointestinal tract contain two distinct cell types, the interstitial cells of Cajal and smooth muscle cells, which together produce rhythmic depolarizations known as slow waves. The bidomain model of tissue-level electrical activity consists of single intracellular and extracellular domains separated by an intervening membrane at all points in space and is therefore unable to adequately describe the presence of two distinct cell types in its conventional form. Here, an extension to the bidomain framework is presented whereby multiple interconnected cell types can be incorporated. Although the derivation is focused on the interactions of the interstitial cells of Cajal and smooth muscle cells, the conceptual framework can be more generally applied. Simulations demonstrating the feasibility of the proposed model are also presented.

INTRODUCTION

The bidomain framework has long been used in the cardiac field to describe tissue- and organ-level electrophysiology, providing the means to link cellular electrical activity to higher-level constructs (1–3). A bidomain is a continuum representation of the underlying tissue with volume-averaged properties over length scales typically larger than a single cell. Each control volume contains two domains, intracellular and extracellular, separated by a membrane that can be considered equivalent to an appropriately scaled outer cell membrane. Detailed discussions of the bidomain framework can be found elsewhere, for example, in Henriquez (4) or Pullan et al. (5).

The conventional bidomain equations are readily applicable to the cardiac field, because most simulations are performed considering only one cell type in the domain of interest. For example, in a block of ventricular muscle, only ventricular myocytes are usually described. Note that this does not imply that myocytes in the domain of interest have the same properties, since spatially varying parameters, such as ion channel densities, can be readily incorporated. The musculature within the walls of the gastrointestinal tract, on the other hand, contains not one but two cell types, the interstitial cells of Cajal (ICCs) and smooth muscle cells (SMCs) (6). Both of these cell types are widely distributed throughout the gastrointestinal musculature and are electrically coupled to themselves and to each other via gap junctions (7,8). It is their combined activity that gives rise to the electrical slow waves that coordinate peristalsis, and therein lies the problem. At the continuum scale on which the bidomain equations operate, any control volume will contain both ICCs and SMCs. The work presented here addresses this issue by describing an extension to the classical bidomain framework that allows multiple cell types to be incorporated. Although the solution is necessarily focused on ICCs and SMCs in the gastrointestinal tract, the concepts behind it are readily applicable and extensible to other similar scenarios.

A relatively limited number of previous modeling studies exist in this area. Aliev et al. developed a dimensionless cable model of electrical activity in the small intestine whereby a reaction-diffusion equation was solved in separate ICC and SMC domains in the absence of axial diffusion in the extracellular space (9). Building on this approach, larger-scale models of gastric and small intestinal electrophysiology have been developed (10,11). In these models, the ICCs and SMCs were placed in separate discrete layers within the walls of the organ of interest. However, it is known that the ICCs are widely distributed within the muscular layers as well as between them (6), calling this approach into question. The absence of an extracellular domain, resulting in a monodomain framework, also removes extracellular coupling as a potential mechanism for cell-cell interaction.

METHODS

Conventional bidomain framework

Before describing the extended bidomain framework, it is useful to consider a brief derivation of the conventional bidomain in equivalent terminology. The starting point selected here is the continuity equation describing the conservation of charge. Because the electrical fields that are generated internally occur at relatively low frequencies (generally <100 Hz), it is common to assume that the system is quasistatic. The continuity equation can subsequently be written as

$$\nabla \cdot \boldsymbol{J} = 0, \tag{1}$$

where $\boldsymbol{J}$ is the current density. This can be divided into two components, one Ohmic, $\boldsymbol{J}_r$, and the other an impressed current density, $\boldsymbol{J}_s$,

$$\boldsymbol{J} = \boldsymbol{J}_r + \boldsymbol{J}_s. \tag{2}$$

Submitted November 10, 2009, and accepted for publication March 16, 2010.

*Correspondence: biebml@nus.edu.sg

Editor: Arthur Sherman.

0006-3495/10/07/0013/6 $2.00

doi: 10.1016/j.bpj.2010.03.054

The Ohmic component is usually expressed in terms of a conductivity, σ, and an electric field intensity, $\boldsymbol{E}$, which in turn can be expressed in terms of the gradient of a scalar potential, ϕ,

$$\boldsymbol{J}_r = \sigma\boldsymbol{E} = -\sigma\nabla\phi. \quad (3)$$

Within a control volume, the potential difference across the cell membrane, V_m, can be expressed as the difference between an intracellular potential, ϕ_i, and an extracellular potential ϕ_e. Given conductivities ϕ_i and ϕ_e in the intra- and extracellular spaces, respectively, and in the absence of any externally applied currents, Eq. 1 can be stated as

$$\nabla\cdot(J_i + J_e) = \nabla\cdot(-\sigma_i\nabla\phi_i + \sigma_e\nabla\phi_e) = 0, \quad (4)$$

where $\boldsymbol{J}_i$ and $\boldsymbol{J}_e$ are the current densities in the intra- and extracellular spaces. Conservation of charge is maintained as the divergence from a given control volume is zero, but charge may be transferred between the intracellular and extracellular spaces within a control volume. To move from one space to the other, however, the charges must cross the membrane that separates these two spaces,

$$\nabla\cdot(\sigma_i\nabla\phi_i) = \nabla\cdot(\sigma_e\nabla\phi_e) = A_m I_m. \quad (5)$$

Here, I_m is the current/unit membrane area that is crossing the membrane and A_m is the surface area of the membrane/unit volume. Current flow across the membrane is usually written in terms of a capacitive component and the sum of any ionic currents that are present,

$$I_m = C_m\frac{\partial V_m}{\partial t} + I_{ion}. \quad (6)$$

In this form, the specific capacitance, C_m, and the ionic current term, I_{ion}, are expressed per unit membrane area. The two bidomain equations can therefore be written as

$$\nabla\cdot(\sigma_i\nabla\phi_i) = A_m\left(C_m\frac{\partial V_m}{\partial t} + I_{ion}\right) \quad (7)$$

$$\nabla\cdot(\sigma_e\nabla\phi_e) = -A_m\left(C_m\frac{\partial V_m}{\partial t} + I_{ion}\right). \quad (8)$$

Extended bidomain framework

The key idea in extending the bidomain framework described above to incorporate multiple cell types is the distribution of the surface area/volume ratio, A_m. In the conventional bidomain framework, this parameter represents the total cell surface area/unit control volume. It can be thought of as a measure of the available area across which ion transport is possible within the control volume. If we consider the situation where both ICCs and SMCs are present, some fraction of the membrane area will be available for ions to be exchanged between the ICCs and the extracellular space, and another fraction will be available for ions to be exchanged between the SMCs and the extracellular space. The ICCs and SMCs are also directly coupled via gap junctions; therefore, there will also be ion transfer between these cell types that does not involve the extracellular space. Given an ICC surface area/unit volume, A_m^{ICC}, an SMC surface area/unit volume, A_m^{SMC}, and an area for ion transfer between the cell types, A_m^{gap}, the surface/volume ratio can be expressed as

$$A_m = A_m^{ICC} + A_m^{SMC} + A_m^{gap}. \quad (9)$$

Henceforth, superscripts ICC and SMC are added to denote parameters relating to the ICCs and SMCs, respectively. In the ICCs, the interaction with the extracellular space will be governed by Eq. 7, thus,

$$\nabla\cdot\left(\sigma_i^{ICC}\nabla\phi_i^{ICC}\right) = A_m^{ICC}\left(C_m^{ICC}\frac{\partial V_m^{ICC}}{\partial t} + I_{ion}^{ICC}\right). \quad (10)$$

In a similar way, the interaction between the SMCs and the extracellular space will be governed by

$$\nabla\cdot\left(\sigma_i^{SMC}\nabla\phi_i^{SMC}\right) = A_m^{SMC}\left(C_m^{SMC}\frac{\partial V_m^{SMC}}{\partial t} + I_{ion}^{SMC}\right). \quad (11)$$

In the shared extracellular space, ionic currents will cross a total membrane area of $A_m^{ICC} + A_m^{SMC}$ and as such will receive contributions from the ICCs and SMCs that are proportional to their relative area fractions and dependent on cellular activity,

$$\nabla\cdot(\sigma_e\nabla\phi_e) = -A_m^{ICC}\left(C_m^{ICC}\frac{\partial V_m^{ICC}}{\partial t} + I_{ion}^{ICC}\right) - A_m^{SMC}\left(C_m^{SMC}\frac{\partial V_m^{SMC}}{\partial t} + I_{ion}^{SMC}\right). \quad (12)$$

As an alternative, Eqs. 10–12 can be combined to express the governing equation for the extracellular space in terms of the continuity equation as

$$\nabla\cdot(\sigma_e\nabla\phi_e) + \nabla\cdot\left(\sigma_i^{ICC}\nabla\phi_i^{ICC}\right) + \nabla\cdot\left(\sigma_i^{SMC}\nabla\phi_i^{SMC}\right) = 0. \quad (13)$$

It should be noted that a conventional bidomain can be easily reconstructed by assigning all of the available membrane area to a single cell type.

The form of the governing equations describes the ICCs and SMCs as two independent syncytia that are indirectly coupled through the extracellular space. In contrast, any ion transfer between the ICCs and SMCs is assumed to be local in nature such that there is a local transfer of charge across the membrane connecting the two syncytia. Given a membrane conductance/unit area, g_{gap}, the current between the ICCs and SMCs is governed by the difference between their intracellular potentials,

$$I_{gap} = g_{gap}\left(\phi_i^{ICC} - \phi_i^{SMC}\right). \quad (14)$$

With an intervening membrane area, A_m^{gap}, Eqs. 10 and 11 become

$$\nabla\cdot\left(\sigma_i^{ICC}\nabla\phi_i^{ICC}\right) = A_m^{ICC}\left(C_m^{ICC}\frac{\partial V_m^{ICC}}{\partial t} + I_{ion}^{ICC}\right) + A_m^{gap}I_{gap} \quad (15)$$

$$\nabla\cdot\left(\sigma_i^{SMC}\nabla\phi_i^{SMC}\right) = A_m^{SMC}\left(C_m^{SMC}\frac{\partial V_m^{SMC}}{\partial t} + I_{ion}^{SMC}\right) - A_m^{gap}I_{gap}. \quad (16)$$

Finally, the means to provide an external stimulus to the system can be included. The cases considered here are a transmembrane current stimulus into the ICCs (I_{stim}^{ICC}), and/or the SMCs (I_{stim}^{SMC}), and a current injection into the extracellular space (I_{stim}^{EXT}). The first two stimuli are applied across the cell membrane and therefore act like ionic currents. For the case of the extracellular current injection, the impressed stimulus current (or current density (Eq. 2)) does not directly cross the cell membrane but may subsequently activate or suppress ion channel activity. Including these stimulation mechanisms, the equations governing the extended bidomain framework can therefore be written as

$$\nabla\cdot\left(\sigma_i^{ICC}\nabla\phi_i^{ICC}\right) = A_m^{ICC}\left(C_m^{ICC}\frac{\partial V_m^{ICC}}{\partial t} + I_{ion}^{ICC} - I_{stim}^{ICC}\right) + A_m^{gap}I_{gap} \quad (17)$$

$$\nabla\cdot\left(\sigma_i^{SMC}\nabla\phi_i^{SMC}\right) = A_m^{SMC}\left(C_m^{SMC}\frac{\partial V_m^{SMC}}{\partial t} + I_{ion}^{SMC} - I_{stim}^{SMC}\right) - A_m^{gap}I_{gap} \quad (18)$$

$$\nabla\cdot(\sigma_e\nabla\phi_e)+\nabla\cdot\left(\sigma_i^{ICC}\nabla\phi_i^{ICC}\right)+\nabla\cdot\left(\sigma_i^{SMC}\nabla\phi_i^{SMC}\right)+I_{stim}^{EXT}=0. \tag{19}$$

The resulting framework is depicted in Fig. 1.

Equations 17–19 contain a mixture of intracellular, extracellular, and transmembrane potentials. It is therefore common to perform further manipulation such that they may be written in a form that is more convenient to deal with computationally. One option is to use the linearity of the Laplace operator, whereby $\nabla\cdot(\sigma_i^{ICC}\nabla\phi_e)$ is both added and subtracted from the left-hand side of Eq. 17. The result is a reaction-diffusion equation for V_m^{ICC} that can be evaluated given an extracellular potential field,

$$\begin{aligned}&\nabla\cdot\left(\sigma_i^{ICC}\nabla V_m^{ICC}\right)+\nabla\cdot\left(\sigma_i^{ICC}\nabla\phi_e\right)\\&\quad=A_m^{ICC}\left(C_m^{ICC}\frac{\partial V_m^{ICC}}{\partial t}+I_{ion}^{ICC}-I_{stim}^{ICC}\right)+A_m^{gap}I_{gap}.\end{aligned} \tag{20}$$

A similar procedure can be applied to Eq. 18 to get a reaction-diffusion equation for V_m^{SMC},

$$\begin{aligned}&\nabla\cdot\left(\sigma_i^{SMC}\nabla V_m^{SMC}\right)+\nabla\cdot\left(\sigma_i^{SMC}\nabla\phi_e\right)\\&\quad=A_m^{SMC}\left(C_m^{SMC}\frac{\partial V_m^{SMC}}{\partial t}+I_{ion}^{SMC}-I_{stim}^{SMC}\right)+A_m^{gap}I_{gap}.\end{aligned} \tag{21}$$

Finally, a Poisson equation to calculate the extracellular potential field from the transmembrane potential fields can be formed by subtracting $\nabla\cdot(\sigma_i^{ICC}\nabla\phi_e)$ and $\nabla\cdot(\sigma_i^{SMC}\nabla\phi_e)$ from both sides of Eq. 19:

$$\begin{aligned}&\nabla\cdot\left(\left(\sigma_e+\sigma_i^{ICC}+\sigma_i^{SMC}\right)\nabla\phi_e\right)+I_{stim}^{EXT}\\&\quad=-\nabla\cdot\left(\sigma_i^{ICC}\nabla V_m^{ICC}\right)-\nabla\cdot\left(\sigma_i^{SMC}\nabla V_m^{SMC}\right).\end{aligned} \tag{22}$$

An alternative formulation can be obtained in terms of ϕ_i^{ICC}, ϕ_i^{SMC}, and ϕ_e by leaving Eq. 19 unchanged and splitting the time derivatives in Eqs. 17 and 18 into their intracellular and extracellular components, as in Eqs. 23 and 24. These expressions can be subsequently rearranged to give expressions for ϕ_i^{ICC} and ϕ_i^{SMC} over time,

$$\begin{aligned}\nabla\cdot\left(\sigma_i^{ICC}\nabla\phi_i^{ICC}\right)&=A_m^{ICC}\left(C_m^{ICC}\left(\frac{\partial\phi_i^{ICC}}{\partial t}-\frac{\partial\phi_e}{\partial t}\right)\right.\\&\quad\left.+I_{ion}^{ICC}-I_{stim}^{ICC}\right)+A_m^{gap}I_{gap}\end{aligned} \tag{23}$$

$$\begin{aligned}\nabla\cdot\left(\sigma_i^{SMC}\nabla\phi_i^{SMC}\right)&=A_m^{SMC}\left(C_m^{SMC}\left(\frac{\partial\phi_i^{SMC}}{\partial t}-\frac{\partial\phi_e}{\partial t}\right)\right.\\&\quad\left.+I_{ion}^{SMC}-I_{stim}^{SMC}\right)-A_m^{gap}I_{gap}.\end{aligned} \tag{24}$$

RESULTS

To test the framework, an implementation was constructed using the second formulation, whereby Eqs. 19, 23, and 24 were discretized using a forward-time, central-space finite difference scheme and assembled into a single matrix system. The Laplacian terms in Eqs. 23 and 24 were calculated implicitly, whereas the ionic and gap junction currents were calculated explicitly. The ICC and SMC ionic current models were taken from Corrias and Buist (12,13). The remaining bidomain model parameters are given in Table 1. It should be noted here that A_m^{gap} and g_{gap} are not independent, and that other combinations whose product is the same would have no effect on the subsequent calculations. The test geometry was a cable of length 100 mm discretized at a resolution of 1 mm. The resulting system of equations was solved using a stabilized biconjugate gradient method

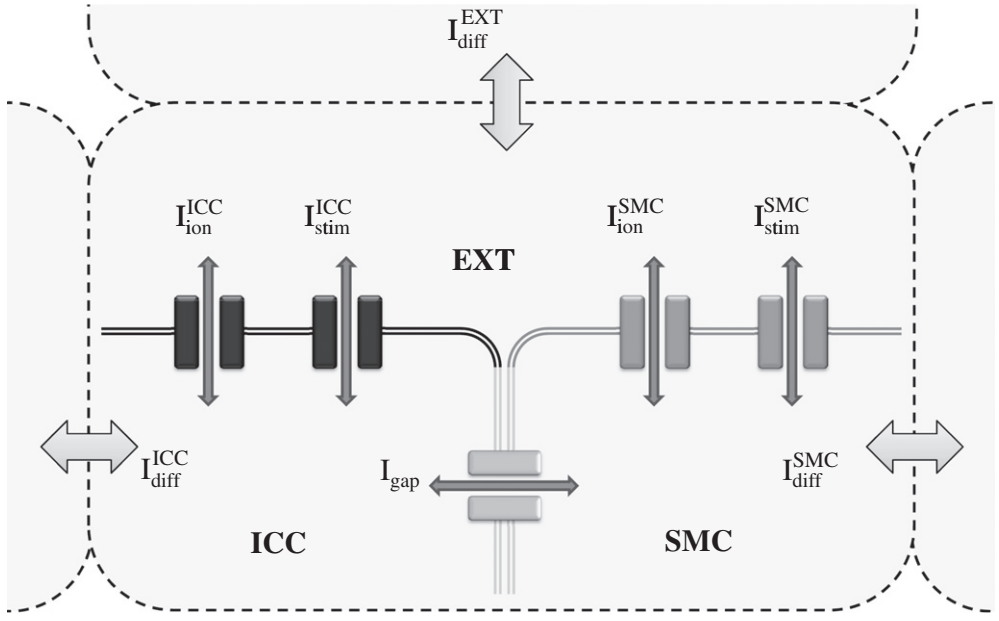

FIGURE 1 Schematic of the extended bidomain framework for a single control volume. Within the control volume, the membrane area available for ion exchange is separated into three components, one for the interaction between the ICC and the extracellular space, one for the interaction between the SMC and the extracellular space, and the third for the interaction between the ICC and the SMC. Currents are defined in the body text with the exception of I_{diff}^{ICC}, I_{diff}^{SMC}, and I_{diff}^{EXT}, which represent $\nabla\cdot(\sigma_i^{ICC}\nabla\phi_i^{ICC})$, $\nabla\cdot(\sigma_i^{SMC}\nabla\phi_i^{SMC})$, and $\nabla\cdot(\sigma_e\nabla\phi_e)$, respectively.

TABLE 1 Bidomain parameter values

Parameter	Value	Units
σ_i^{ICC}	0.5	mS.mm^{-1}
σ_i^{SMC}	0.1	mS.mm^{-1}
σ_e	0.1	mS.mm^{-1}
C_m^{ICC}	0.01	μF.mm^{-2}
C_m^{SMC}	0.01	μF.mm^{-2}
A_m^{ICC}	100	mm^{-1}
A_m^{SMC}	100	mm^{-1}
A_m^{gap}	0.1	mm^{-1}
g_{gap}	0.2	mS.mm^{-2}

with a time step of 0.1 ms. In the absence of any essential boundary conditions, the solution of the resulting system of equations is only unique up to an arbitrary additive constant. Therefore, to constrain the solution, the average of the extracellular potential field was set to zero.

One of the potential applications of this framework is the simulation of external gastric pacemakers; thus, simulations were performed to test slow-wave entrainment in response to external stimuli. A periodic external stimulus current with duration 200 ms was injected through either I_{stim}^{ICC} or I_{stim}^{EXT} at a frequency of 3.3 cycles/min (cpm) into a system whereby the natural ICC pacing frequency was 2.9 cpm. Entrainment was rapid, and both stimulus methods produced stable slow-wave entrainment at the pacing frequency. The representative traces shown in Fig. 2 were obtained after 45 min of continuous entrainment.

It is interesting that although the stimulus directed into the ICCs reduced the amplitude and duration of the resulting slow waves with the increase in cycling rate, the stimuli injected into the extracellular space increased the amplitude and duration of the slow waves. One possible explanation for this is that under physiological conditions, the SMCs act largely as a passive load on the ICCs. When current is injected into the extracellular space, this burden on the ICCs is reduced. Thus, the ICC waveform displays increased amplitude and, consequently, an increased duration. A similar phenomenon was seen when the stimulus current was injected into the SMCs (data not shown).

Fig. 3 shows a spatiotemporal plot of the ICC and SMC transmembrane potential fields (calculated as the difference between the appropriate intracellular field and the extracellular field) and the extracellular field in the absence of any external stimulus. As the ICCs are self-pacing, slow waves can be seen propagating along the cable, i.e., from top to bottom in Fig. 3. Also displayed are the two transmembrane potential fields and the extracellular potential field as a function of time from one location halfway along the cable. The morphology of the transmembrane potential waves is consistent with that reported previously (14,15). It should be noted that the shape of the extracellular potential field, but not that of the transmembrane potential fields, will depend on the nature of the reference potential constraint that is used.

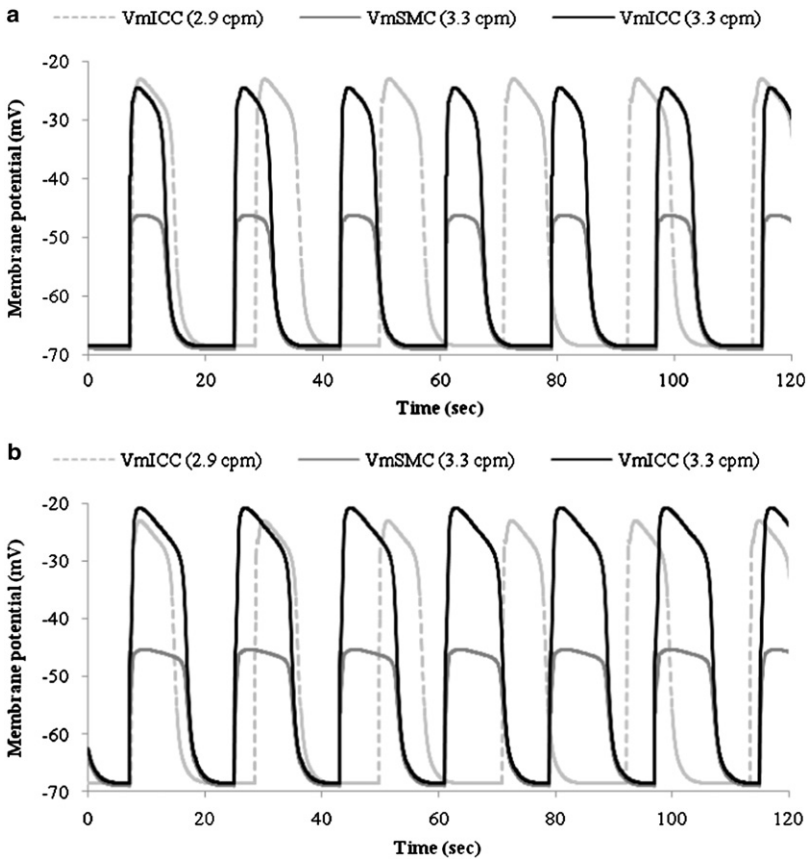

FIGURE 2 Current injection into an extended bidomain framework, showing the unstimulated ICC membrane potential at the intrinsic frequency of 2.9 cpm (*gray dashed lines*), the ICC membrane potential at the stimulated frequency of 3.3 cpm (*solid black lines*), and the SMC membrane potential at 3.3 cpm (*solid gray lines*). (*a*) The result of injecting a periodic stimulus at 3.3 cpm into an ICC via I_{stim}^{ICC}. (*b*) The result of injecting a stimulus into the extracellular space via I_{stim}^{EXT}. Stimuli in both *a* and *b* are able to produce stable entrainment.

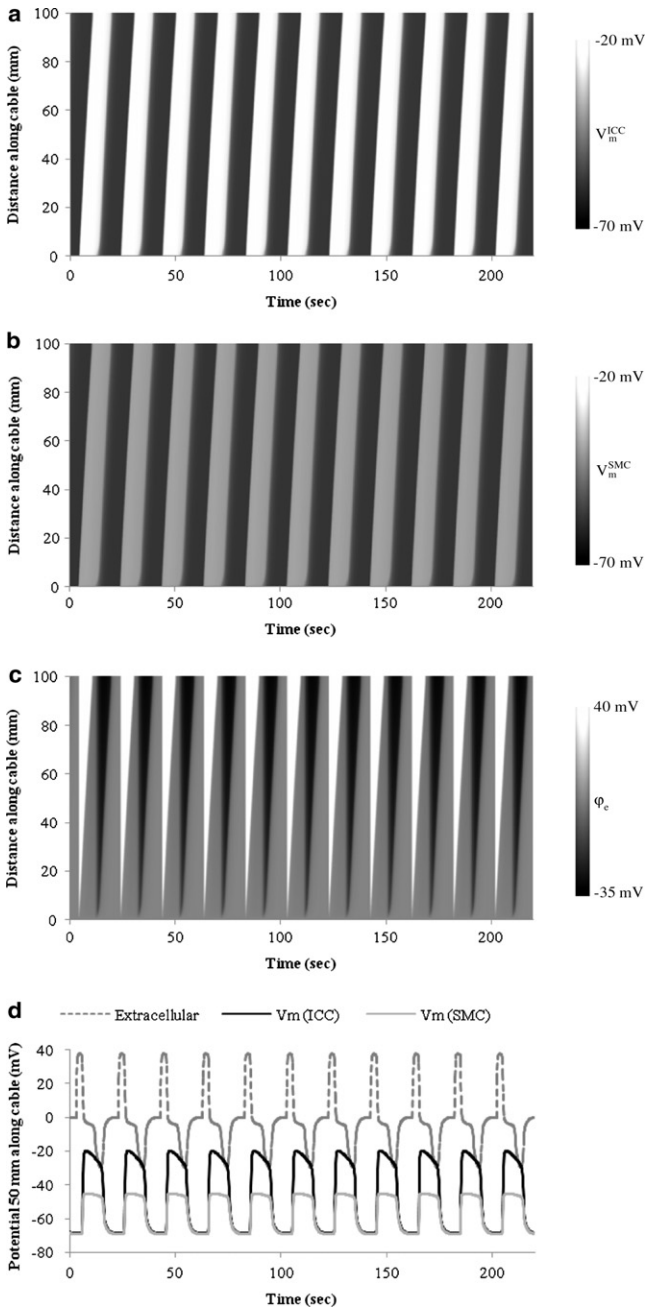

FIGURE 3 (*a–c*) Spatiotemporal plots of voltages V_m^{ICC}, V_m^{SMC}, and ϕ_e, respectively. In each case, the distance along the cable is plotted on the vertical axis, and time is shown on the horizontal axis. The proximal end of the cable is depicted as a distance of zero and the distal end as a distance of 100. Propagation along the cable is therefore observed by activity that moves to the right in time and distally (upward) in space. Here, the extracellular potential at the proximal end of the cable has been grounded to a value of 0 mV for all time. (*d*) The three voltages described in *a–c* as a function of time from a location halfway (50 mm) along the cable.

DISCUSSION

Although this framework has been designed to represent the presence of ICCs and SMCs in the musculature of the gastrointestinal tract, the underlying idea of distributing the membrane surface area among the different cell types in a control volume can be generally applied. Within the gastrointestinal tract, for example, there exists an enteric nervous system that provides an additional local control system. As more quantitative information becomes available, this could be added as a third syncytium within this framework, capable of transmitting information and interacting locally with both ICCs and SMCs. It is interesting that ICC-like cells have also been identified in a number of other tissues, including the heart (16), myometrium (17), and pancreas (18).

In the stomach of many species, a layer of ICCs is located at the myenteric plexus between the longitudinal and smooth muscle layers (ICC-MY), and in the small intestine there is an additional layer in the deep muscular plexus (ICC-DMP). Here, it may be advantageous to form a layer that does not contain SMCs. As mentioned earlier, such a task is quite straightforward, as all that is required is to assign all of A_m to the ICC-MY. If their neural innervations are to be included, these layers can be constructed by describing the presence of the neural and ICC membranes only.

One other potential complication arises because within the musculature there may also be intramuscular ICCs (ICC-IM) whose properties differ from the ICCs in the myenteric plexus (and the ICC-DMP, where applicable). At present, there is insufficient information about how these cell types differ to make a determination of the best approach. However, should their basic mechanisms be sufficiently similar, it is possible to simply add a spatial variation to some of the parameters, e.g., ion channel densities. If not, then the ICC-MY could be constructed from that cell type, whereas the muscle layers could be constructed from the ICC-IM and the SMC.

As mentioned earlier, the parameters governing the strength of the coupling between the ICCs and the SMCs, A_m^{gap} and g_{gap}, are not independent in the formulation of I_{gap}. Simulations were therefore undertaken to determine the sensitivity of the model to this parameter combination. Reducing or enhancing the coupling by a factor of 2 had little effect on the resulting slow-wave activity. As the coupling was reduced to zero, the SMC activity remained nonzero, indicating that current was able to flow to the SMCs from the ICCs via the extracellular space. The resulting activity was, however, of a markedly lower amplitude than a normal slow wave and thus would be unlikely to cause a mechanical contraction. When the coupling was increased substantially from that stated in Table 1, the amplitude of the ICC waveform decreased and became more triangular in shape, whereas the amplitude of the SMC slow wave increased. However, a high coupling regime was not sustainable over the long term, as the ICC waveform gradually decreased in size, presumably due to the increased load from the SMCs, and pacemaker activity eventually ceased.

Funding support from the Ministry of Education Academic Research Fund (grant T13-0902-P02) is gratefully acknowledged.

REFERENCES

1. Sepulveda, N. G., B. J. Roth, and J. P. Wikswo, Jr. 1989. Current injection into a two-dimensional anisotropic bidomain. *Biophys. J.* 55:987–999.
2. Keener, J. P., and A. V. Panfilov. 1996. A biophysical model for defibrillation of cardiac tissue. *Biophys. J.* 71:1335–1345.
3. Li, W., V. Gurev, …, N. A. Trayanova. 2008. The role of mechanoelectric feedback in vulnerability to electric shock. *Prog. Biophys. Mol. Biol.* 97:461–478.
4. Henriquez, C. S. 1993. Simulating the electrical behavior of cardiac tissue using the bidomain model. *Crit. Rev. Biomed. Eng.* 21:1–77.
5. Pullan, A. J., L. K. Cheng, and M. L. Buist. 2005. Mathematically Modelling the Electrical Activity of the Heart. World Scientific, London.
6. Hirst, G. D. S., and F. R. Edwards. 2006. Electrical events underlying organized myogenic contractions of the guinea pig stomach. *J. Physiol.* 576:659–665.
7. Hanani, M., G. Farrugia, and T. Komuro. 2005. Intercellular coupling of interstitial cells of cajal in the digestive tract. *Int. Rev. Cytol.* 242:249–282.
8. Wang, Y. F., and E. E. Daniel. 2001. Gap junctions in gastrointestinal muscle contain multiple connexins. *Am. J. Physiol. Gastrointest. Liver Physiol.* 281:G533–G543.
9. Aliev, R. R., W. Richards, and J. P. Wikswo. 2000. A simple nonlinear model of electrical activity in the intestine. *J. Theor. Biol.* 204:21–28.
10. Buist, M. L., L. K. Cheng, …, A. J. Pullan. 2006. Multiscale modelling of human gastric electric activity: can the electrogastrogram detect functional electrical uncoupling? *Exp. Physiol.* 91:383–390.
11. Lin, A. S. H., M. L. Buist, …, A. J. Pullan. 2006. Modelling slow wave activity in the small intestine. *J. Theor. Biol.* 242:356–362.
12. Corrias, A., and M. L. Buist. 2008. Quantitative cellular description of gastric slow wave activity. *Am. J. Physiol. Gastrointest. Liver Physiol.* 294:G989–G995.
13. Corrias, A., and M. L. Buist. 2007. A quantitative model of gastric smooth muscle cellular activation. *Ann. Biomed. Eng.* 35:1595–1607.
14. Hirst, G. D., and F. R. Edwards. 2001. Generation of slow waves in the antral region of guinea-pig stomach—a stochastic process. *J. Physiol.* 535:165–180.
15. Ward, S. M., R. E. Dixon, …, K. M. Sanders. 2004. Voltage-dependent calcium entry underlies propagation of slow waves in canine gastric antrum. *J. Physiol.* 561:793–810.
16. Popescu, L., M. Gherghiceanu, …, E. Mandache. 2007. Insights into the interstitium of ventricular myocardium: interstitial Cajal-like cells (ICLC). *J. Cell. Mol. Med.* 10:429–458.
17. Ciontea, S. M., E. Radu, …, L. M. Popescu. 2007. C-kit immunopositive interstitial cells (Cajal-type) in human myometrium. *J. Cell. Mol. Med.* 9:407–420.
18. Popescu, L. M., M. E. Hinescu, …, C. Ardelean. 2007. Interstitial cells of Cajal in pancreas. *J. Cell. Mol. Med.* 9:169–190.